Nanostructured Cobalt Oxide Clusters in Mesoporous Silica as Efficient Oxygen-Evolving Catalysts

Feng Jiao and Heinz Frei[#*]

Physical Biosciences Division, Lawrence Berkeley National Laboratory, University of California, Berkeley, CA 94720

[#] This work was funded by the Helios Solar Energy Research Center, which is supported by the Director, Office of Science, Office of Basic Energy Sciences of the U.S. Department of Energy under Contract No. DE-AC02-05CH11231. The authors acknowledge the support of the National Center for Electron Microscopy, Lawrence Berkeley National Laboratory, which is supported by the U.S. Department of Energy. Portions of this research were carried out at the Stanford Synchrotron Radiation Laboratory, a national user facility operated by Stanford University on behalf of the U.S. Department of Energy, Office of Basic Energy Sciences. The SSRL Structural Molecular Biology Program is supported by the Department of Energy, Office of Biological and Environmental Research, and by the National Institutes of Health, National Center for Research Resources, Biomedical Technology Program.

The development of integrated artificial photosynthetic systems for the direct conversion of carbon dioxide and water to fuel depends on the availability of efficient and robust catalysts for the chemical transformations. Catalysts need to exhibit turnover frequency (TOF) and density (hence size) commensurate with the solar flux at ground level (1000 W m^{-2}, AM 1.5)[1] in order to avoid wasting of incident solar photons. For example, a catalyst with a TOF of 100 s^{-1} requires a density of one catalytic site per nm^2. Catalysts with lower rates or taking up a larger space will require a high surface area, nanostructured support that affords tens to hundreds of catalytic sites nm^{-2}. Furthermore, catalysts need to operate close to the thermodynamic potential of the redox reaction so that a maximum fraction of the solar photon energy is converted to chemical energy. Stability considerations favor all-inorganic oxide materials, as do avoidance of harsh reaction conditions of pH or temperature.

For the water oxidation half reaction, Ir oxide is a material that essentially fulfils these requirements. Following early reports which identified IrO_2 particles as robust water oxidation catalysts [2-4], Mallouk determined a TOF for Ir oxide colloidal particles of 40 s^{-1} in aqueous solution (pH 5.7, 25 ^oC), most recently for particles as small as 2 nm.[5-7] In this work, the catalyst was driven by $Ru^{+3}(bpy)_3$ generated photochemically with visible light using the established $Ru^{+2}(bpy)_3$-persulfate system, with a modest overpotential (η) of 370 mV. For IrO_2 colloidal particles coated on an indium tin oxide anode, Yagi obtained TOF = 7 s^{-1} (pH 5.3, 25 ^oC, η = 570 mV) from electrochemical measurements.[8] We have recently demonstrated that all-inorganic photocatalytic units consisting of nanoclusters (approx. 2 nm) directly coupled to a single center Cr^{VI} [9] or a

binuclear $TiCr^{III}$ [10] charge-transfer chromophore afford oxygen evolution under visible light with good quantum yield. While Ir oxide closely approaches the efficiency and stability required for a water oxidation catalyst in a solar conversion system, it is the least abundant metal on earth and not suitable for use on a very large scale. Therefore, it is imperative to explore oxides of the much more abundant first row transition metals, as inspired by Nature's Mn_4Ca cluster of Photosystem II.[11] In this paper, we focus Co oxide nanoclusters as candidates for water oxidation catalysts under mild conditions.

Numerous electrochemical studies of Co and Mn oxides as catalytic materials for oxygen evolution have been conducted over the past decades. For the purpose of evaluating metal oxides in the form of nanosized clusters as catalytic components for water oxidation, comparisons of turnover frequencies are most relevant. Such values were typically not reported in electrochemical studies, but lower limits can be calculated in cases where the amount of catalyst material was communicated in the respective paper. The data are summarized in Table 1 of the Supporting Information ('lower limits' refers to the assumption that all deposited metal centers are catalytically active).[12] Briefly, for Co_3O_4 (spinel) lower limits of TOF ranging from 0.020 to 0.0008 s^{-1} at high pH and temperatures between 25 and 120 ^oC were derived from work by Schmidt [13], Iwakura [14], and Rasiyah et al.[15]. Overpotentials range between 300 and 400 mV. While these electrochemical measurements were conducted in alkaline solution to maximize rates, less harsh conditions are preferable for artificial photosynthetic systems for reasons of structural stability. Using an established *in-situ* activation method for developing a Co-based electrocatalytic film [13], Kanan and Nocera reported very recently oxygen

evolution from pH neutral, phosphate-buffered aqueous solution (room temperature, current density 1 mA cm^{-2}, η = 410 mV).[16] While the exact formula and density of the catalyst were not reported, the thickness of the Co phosphate layer of about 2 μ and the observed current density allow an estimate of TOF $\geq$ 0.0007 s^{-1} if a density of Co centers in the electrocatalytic film equal to that of $Co_3(PO_4)_2$ is assumed. A study at neutral pH and room temperature using an anode coated with MnO_2 by Morita et al. gave TOF $\geq$ 0.013 s^{-1} (η = 440 mV).[17] In addition, oxygen evolution was reported by Harriman et al. from aqueous suspensions of micrometer sized Co_3O_4 or Mn_2O_3 particles using the photo-chemical $Ru^{+2}(bpy)_3$ - persulfate method (pH 5, room temperature, η = 325 mV)).[4] Data presented in the paper indicate TOF between 0.035 and 0.055 s^{-1}. The photochemical and electrochemical results of Co and Mn oxides clearly suggest that these materials hold promise for developing robust, efficient nanometer sized catalysts for water oxidation. Here we report efficient oxygen evolution at nanometer sized Co_3O_4 clusters in mesoporous silica in aqueous solution under mild temperature and pH conditions for the first time. The catalyst was driven by the $Ru^{+2}(bpy)_3$ – persulfate sensitizer system under visible light.

Typical TEM images of Co oxide nanoclusters prepared in SBA-15 silica [18] at 4.2 wt% and 8.6 wt% loading (per ICP-MS) by wet impregnation are shown in Figure 1(a) and (b), respectively.[12,19,20] The images show that the integrity of the silica channel structure (diameter 8 nm) was maintained upon formation of the Co oxide clusters. By examining many SBA-15 particles in different regions of the powder, we confirmed that Co oxide nanoclusters are formed exclusively inside the mesopores; no

clusters were found on the outer surface of the silica particles. The oval shaped clusters consist of parallel bundles of nanorods whose structure is imposed by the silica channels. The rods are linked by short bridges, formed by Co oxide growth in the micropores interconnecting the mesoscale channels.[19] TEM images of the Co oxide clusters obtained after removal of the silica scaffold by heating of a suspension of the SBA-15/Co oxide (4%) sample in aqueous NaOH (2 M) at 60^{o}C for 30 min are shown in Figure 1(c). Analysis of hundreds of clusters shows that the average Co oxide cluster is oval-shaped and spans four nanorods, which corresponds to a diameter of 35 nm (histogram analysis shown in Figure S2).[12] For the 8% sample, the average bundle of nanorods spans 100 nm (Figure 1b).

Selected area electron diffraction (SAED) images shown in the inset of Figure 1b confirm the crystalline nature of the 100 nm Co oxide nanoclusters. By contrast, no clear diffraction pattern was observed for the 4% sample, suggesting that the 35 nm clusters are poorly crystallized. These findings are confirmed by powder X-ray diffraction (XRD) measurements shown in Figure 2. The diffraction peaks of the bulk Co oxide phase (trace a) are characteristic for Co_3O_4 (spinel structure).[21] The same peaks are clearly visible in the pattern of the 100 nm Co oxide clusters of the 8% sample (trace c), but absent in the 4% sample (trace b). The absence of diffraction peaks for the 35 nm clusters indicates that the crystalline domains are very small (at most a few nm) and points to polycrystallinity of the clusters. The width of the XRD bands in the case of the 8% sample corresponds to a 7.6 nm object according to the Scherrer formula, in agreement with the expected diameter of Co oxide nanorods imposed by the SBA-15 channel

structure (Figure 1). Fourier-transformed EXAFS data for micron-sized Co_3O_4 particles and Co_3O_4 nanoclusters of 8% and 4% loaded SBA-15 are shown in Figure 3. The perfect agreement between the spectra of bulk Co_3O_4 (black trace) and SBA-15/Co_3O_4(8%) (red) confirms the well crystallized spinel structure of the 100 nm clusters, consistent with the SAED and powder XRD results. For the 4% sample (blue), there is good agreement between the first shell Co-O bond distances for the nanoclusters and the bulk phase. The higher shell Co-Co peaks, while clearly visible, have much lower intensity indicative of very small (few nm) crystalline Co_3O_4 domains within the 35 nm cluster. Precedents for reduced EXAFS peak intensities due to polycrystallinity have been reported previously.[22] We conclude that the structural characterization reveals spherically shaped bundles of parallel Co_3O_4 nanorods of spinel structure inside the porous SBA-15 scaffold.

Evolution of O_2 was observed by mass spectrometric monitoring of the gas in the head space of aqueous suspensions of SBA-15/Co_3O_4 catalysts driven by visible light-generated $Ru^{+3}(bpy)_3$ at pH 5.8 and room temperature (476 nm, 240 mW), as shown in Figure 4, trace c and d. A mildly acidic pH was chosen in order to minimize photodegradation of the Ru complex.[23] The amount of O_2 generated increases approximately linearly for the first 30 minutes before gradually leveling off. When adding fresh $Na_2S_2O_8$ acceptor and readjusting the pH to 5.8, oxygen evolution resumed at the same rate within uncertainties as observed initially. This confirms that the slowdown of the water oxidation rate is due to the stoichiometric consumption of the persulfate acceptor and demonstrates that the activity of the Co_3O_4 nanoclusters does not

degrade during photocatalysis on the time scale investigated (several hours). XANES and EXAFS analysis of the Co_3O_4 clusters before and after photochemical runs did not reveal any structural or oxidation state changes of the catalyst (see Supporting Information).[12] The stability of the Co oxide catalyst was further confirmed by the absence of significant leaching of Co ions during photolysis; ICP-MS analysis of solutions after photolysis contained at most 20 ppm Co ions (0.32 μg mL^{-1}). A photochemical experiment with an aqueous solution of such a small amount of Co ions was conducted and no O_2 evolution detected. In a further control experiment, NiO was prepared in SBA-15 at the same loading level (8%) [12] and photolysis was conducted under conditions identical to those used for the SBA-15/Co_3O_4 samples. As can be seen from Figure 4a, no O_2 evolution was detected confirming that Co_3O_4 nanoclusters are responsible for water oxidation. We conclude that Co_3O_4 nanoclusters of spinel structure in SBA-15 silica material exhibit strong oxygen evolution activity under mild pH and temperature conditions, at an overpotential of 350 mV ($\varepsilon^o(Ru^{+3}(bpy)_3/Ru^{+2}(bpy)_3)$ = 1.24 V [24], $\varepsilon^o(O_2/H_2O)$ = 0.89 V at pH 5.8).

While the modest overpotential for driving the catalyst implies reasonable thermodynamic efficiency, the turnover frequency (number of oxygen molecules per second per nanocluster) and size of the catalyst determine the degree to which an integrated system featuring this catalyst will be able to keep up with the rate of incident solar photons. From the amount of O_2 gas evolved in the headspace during the first 10 min of photolysis (Figure 4), taking into account the equilibrium oxygen concentration in the solution volume [9], we estimate a TOF = 1140 s^{-1} per Co_3O_4 nanocluster. The

calculation is based on the cylindrical shape of the bundles of Co oxide nanorods evident from Figure 1c (bundle diameter 35 nm, rod diameter 7.6 nm, average of 14 rods per bundle of 50 nm average length), the loading of 8.4 mg and the density of Co_3O_4 of 6.07 mg cm^{-3}. We conclude that values for turnover frequency and size of the Co oxide nanoclusters on SBA-15 (4% loading) lie in a range adequate for quantitative use of photons at maximum solar intensity. For the larger, 100 nm Co oxide clusters of the SBA-15/Co_3O_4(8%) catalyst, the estimated TOF is 6300 s^{-1}. The calculation assumes a cylindrical geometry of the Co oxide nanorod bundles of 100 nm diameter (average of rods 115 nanorods per bundle, rod diameter 7.6 nm, average length 100 nm).

As can be seen from Figure 4, the oxygen yield is 65 times smaller for an aqueous suspension of bare Co_3O_4 particles of micron (trace b) compared to that of the nanoclusters of SBA-15/Co_3O_4(4%), and 40 times smaller than for the SBA-15/Co_3O_4(8%) sample. The fact that the total amount of Co oxide of the micron-sized particle sample exceeds that of the SBA-15/Co_3O_4(8%) sample by a factor of 12 indicates that Co centers in the interior of the particles or clusters are not involved in the catalysis. A comparison of the number of surface Co sites for the micrometer-sized particles and the nanoclusters points to the important role of surface Co centers. Assuming the geometry for the particles and nanoclusters described above and taking as nanocluster surface the combined surface area of all nanorods of the bundle (16 percent of the Co is at the surface), we calculate that the ratio of surface Co centers of the Co_3O_4 nanocluster sample to μ-sized Co_3O_4 sample is 13 in the case of SBA-15/Co_3O_4(4%), or 26 for SBA-15/Co_3O_4(8%) (it is interesting to note that spherical Co_3O_4 particles of the same size as

the nanorod bundles but without the nanorod structure would have about the same surface area as the sample of μ sized particles). These estimates suggest that the much larger surface area provided by the internal nanorod structure of the Co_3O_4 clusters is an important factor contributing to the high TOF of the nanoclusters. However, it seems not to account for the high TOF completely because the O_2 yield difference exceeds the surface area factor significantly. Therefore, in addition, Co surface sites of nanoclusters may be more efficient catalytically than those of μ sized particles.[25] The lower O_2 product yield for the SBA-15/Co_3O_4(8%) compared to the SBA-15/Co_3O_4(4%) sample (Figure 4) despite the two times larger total number of surface Co of the former may signal less efficient access of the reactant to the surface of individual nanorods in the case of the much larger, 100 nm nanorod bundles.

The quantum efficiency of the $Ru^{+2}(bpy)_3$ – persulfate system used here for driving the water oxidation catalyst is calculated as 18% for the SBA-15/Co_3O_4(4%) experiment (2 times the number of O_2 molecules produced divided by number of photon absorbed by the sensitizer).[4] This quantum yield is only a lower limit because it is assumed that all photons are absorbed by the sensitizer in the strongly scattering suspension, which is an overestimation. The value is influenced by several factors including the efficiency of electron transfer between the excited $Ru^{+2}(bpy)_3$ sensitizer and the $S_2O_8^{2-}$ acceptor, and the efficiency of charge transfer between Co_3O_4 nanocluster and $Ru^{+3}(bpy)_3$ inside the silica mesopores. Hence, it may depend on the particular sensitizer used for driving the catalyst. Note that the turnover frequencies were not limited by the

visible light intensity in the experiments reported here and are therefore intrinsic properties of the Co oxide catalysts.

In preliminary experiments using the same sample preparation methods and oxygen evolution measurements, we have observed water oxidation activities for Mn_2O_3 and MnO_2 nanoclusters in SBA-15 similar to those of SBA-15/Co_3O_4. These results will be reported in a forthcoming paper.

In conclusion, oxygen evolution at nanostructured Co_3O_4 clusters in mesoporous silica reported here constitutes the first observation of efficient water oxidation by a nanometer sized multi-electron catalyst made of a first row transition metal oxide. Rates and size of the catalyst are comparable to nature's Photosystem II, where the majority of the space is taken up by the light harvesting system rather than the catalyst. The abundance of the metal oxide, the stability of the nanoclusters under use, the modest overpotential and mild pH and temperature conditions make this a promising catalytic component for developing a viable integrated solar fuel conversion system, the next important challenge in this field.

References

[1] http://rredc.nrel.gov/solar/spectra/am1.5

[2] Kiwi, J.; Gratzel, M. *Angew. Chem. Int. Ed.* **1978**, *11*, 860-861.

[3] Lehn, J.M.; Sauvage, J.P.; Ziessel, R. *Nouv. J. Chim.* **1980**, *4*, 355-358.

[4] Harriman, A.; Pickering, I.J.; Thomas, J.M.; Christensen, P.A. *J. Chem. Soc., Farad. Trans. 1* **1988**, *84*, 2795-2806.

[5] Hara, M.; Lean, J.T.; Mallouk, T.E. *Chem. Commun.* **2001**, *13*, 4668-4675.

[6] Morris, N.D.; Suzuki, M.; Mallouk, T.E. *J. Phys. Chem. A* **2004**, *108*, 9115-9119.

[7] Hoertz, P.G.; Kim, Y.I.; Youngblood, W.J.; Mallouk, T.E. *J. Phys. Chem. B* **2007**, *111*, 6845-6856.

[8] Yagi, M.; Tomita, E.; Sakita, S.; Kuwabara, T.; Nagai, K. *J. Phys. Chem. B* **2005**, *109*, 21489-21491.

[9] Han, H.; Frei, H. *J. Phys. Chem. C* **2008**, *112*, 16156-16159.

[10] Nakamura, R.; Frei, H. *J. Am. Chem. Soc.* **2006**, *128*, 10668-10669.

[11] Yano, J.; Kern, J.; Sauer, K.; Latimer, M.J.; Pushkar, Y.; Biesiadka, J.; Loll, B.; Saenger, W.; Messinger, J.; Zouni, A.; Yachandra, V.K. *Science* **2006**, *314*, 821-825.

[12] Supporting Information

[13] Schmidt, T.; Wendt, H. *Electrochim. Acta* **1994**, *39*, 1763-1767.

[14] Iwakura, C.; Honji, A.; Tamura, H. *Electrochim. Acta* **1981**, *26*, 1319-1326.

[15] Rasiyah, P.; Tseung, A.C.C. *J. Electrochem. Soc.* **1983**, *130*, 365-368.

[16] Kanan, M.W.; Nocera, D.G. *Science* **2008**, *321*, 1072-1075.

[17] Morita, M.; Iwakura, C.; Tamura, H. *Electrochim. Acta* **1977**, *22*, 325-328.

[18] Zhao, D.Y.; Feng, J.L.; Huo, Q.S.; Melosh, N.; Fredrickson, G.H.; Chmelka, B.F.; Stucky, G.D. *Science* **1998**, *279*, 548-

[19] Jiao, F.; Shaju, K.M.; Bruce, P.G. *Angew. Chem. Int. Ed.* **2005**, *44*, 6550-6553

[20] Tian, B.Z.; Liu, X.Y.; Yang, H.F.; Xie, S.H.; Yu, C.Z.; Tu, B.; Zhao, D.Y. *Adv. Mater*. **2003**, *15*, 1370-1374.

[21] Lit XRD of Co_3O_4

[22] Lit on EXAFS peak intensity reduction caused by polycrystallinity

[23] Hara, M.; Waraksa, C.C.; Lean, J.T.; Lewis, B.A.; Mallouk, T.E. *J. Phys. Chem. A* **2000**, *104*, 5275-5280.

[24] *CRC Handbook of Chemistry and Physics, 85th ed.;* Lide, D.R., Editor; CRC Press: Boca Raton, 2004; p. 8-27.

[25] While we observed a very small amount of oxygen evolution for micrometer-sized Co_3O_4 particles upon photolysis using experimental procedures identical to those described in the literature (Ref. 4), we did not observe the much higher water oxidation rates reported by the previous authors.

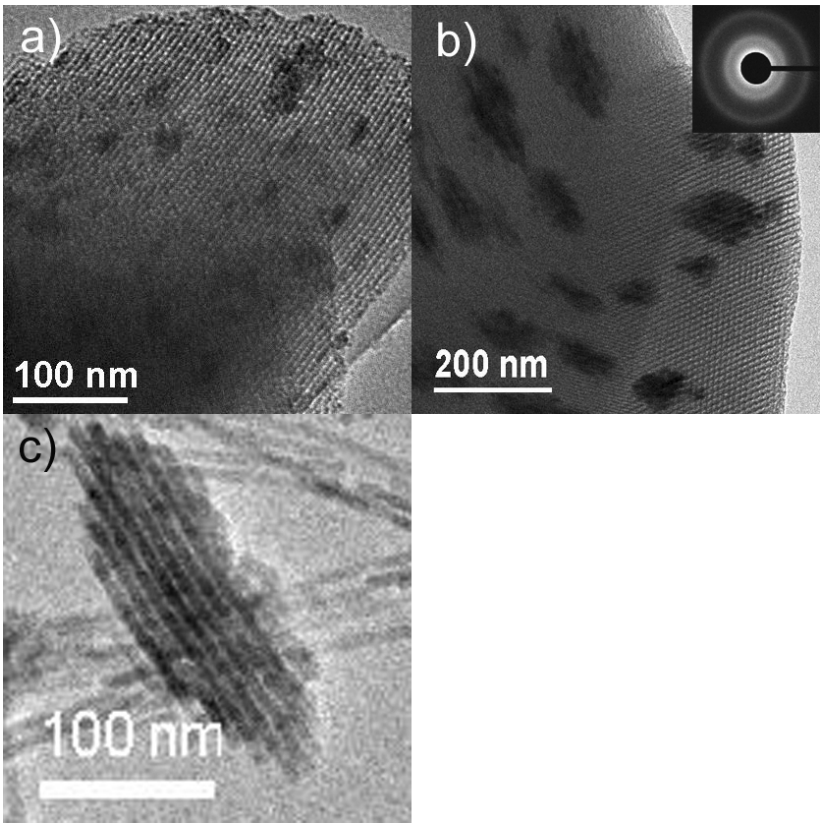

Figure 1: TEM images of (a) SBA-15/Co_3O_4 4% loading. (b) SBA-15/Co_3O_4 8% loading. (c) Co_3O_4 nanoclusters (8% sample) after removal of the SBA-15 silica material using aqueous NaOH as edging reagent. Analysis of the parallel nanorod bundles reveals an average bundle diameter of 35 nm containing 14 nanorods. The shape indicates that the average bundle has 4 nanorods of 80 nm, 4 nanorods of 60 nm, and 6 nanorods of 25 nm length. Hence, the average nanorod length is 50 nm.

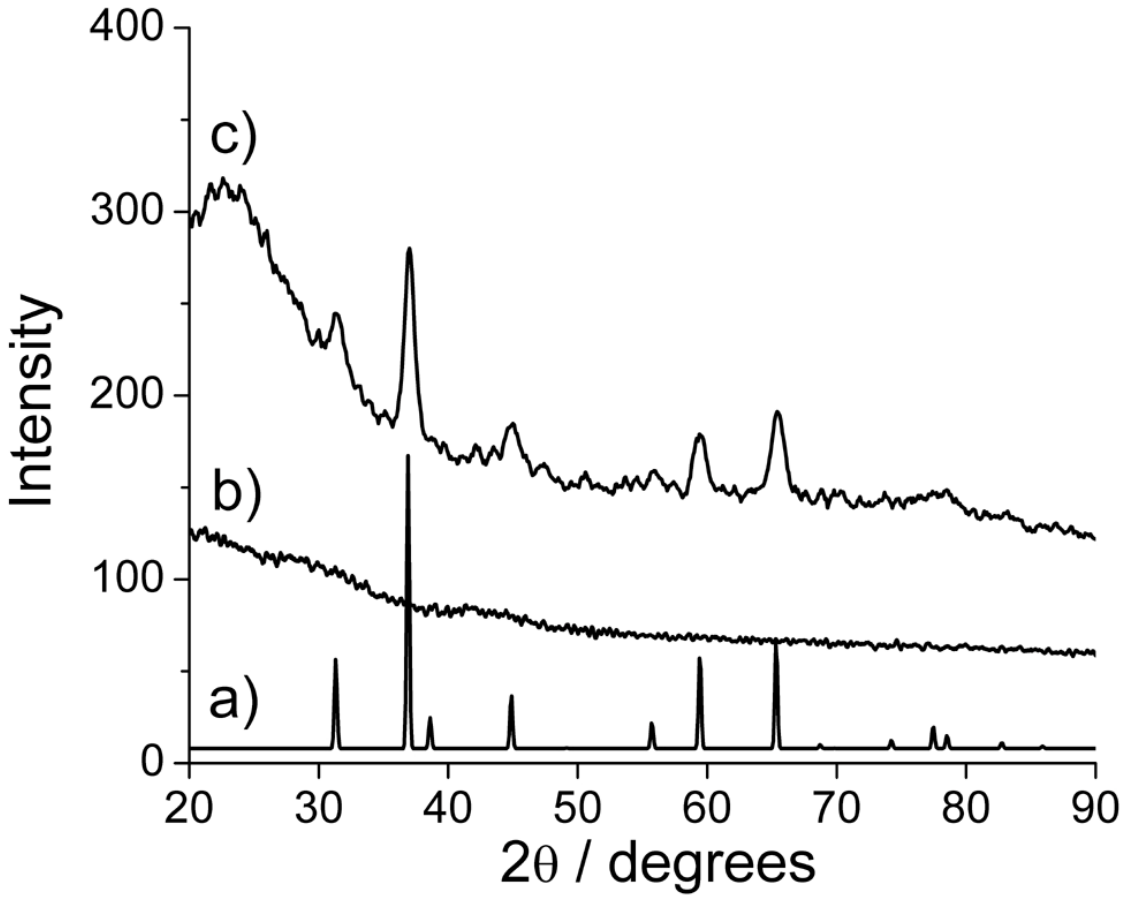

Figure 2: Wide-angle powder XRD patterns for (a) micrometer sized Co_3O_4 particles, (b) SBA-15/Co_3O_4 (4%), (c) SBA-15/Co_3O_4 (8%).

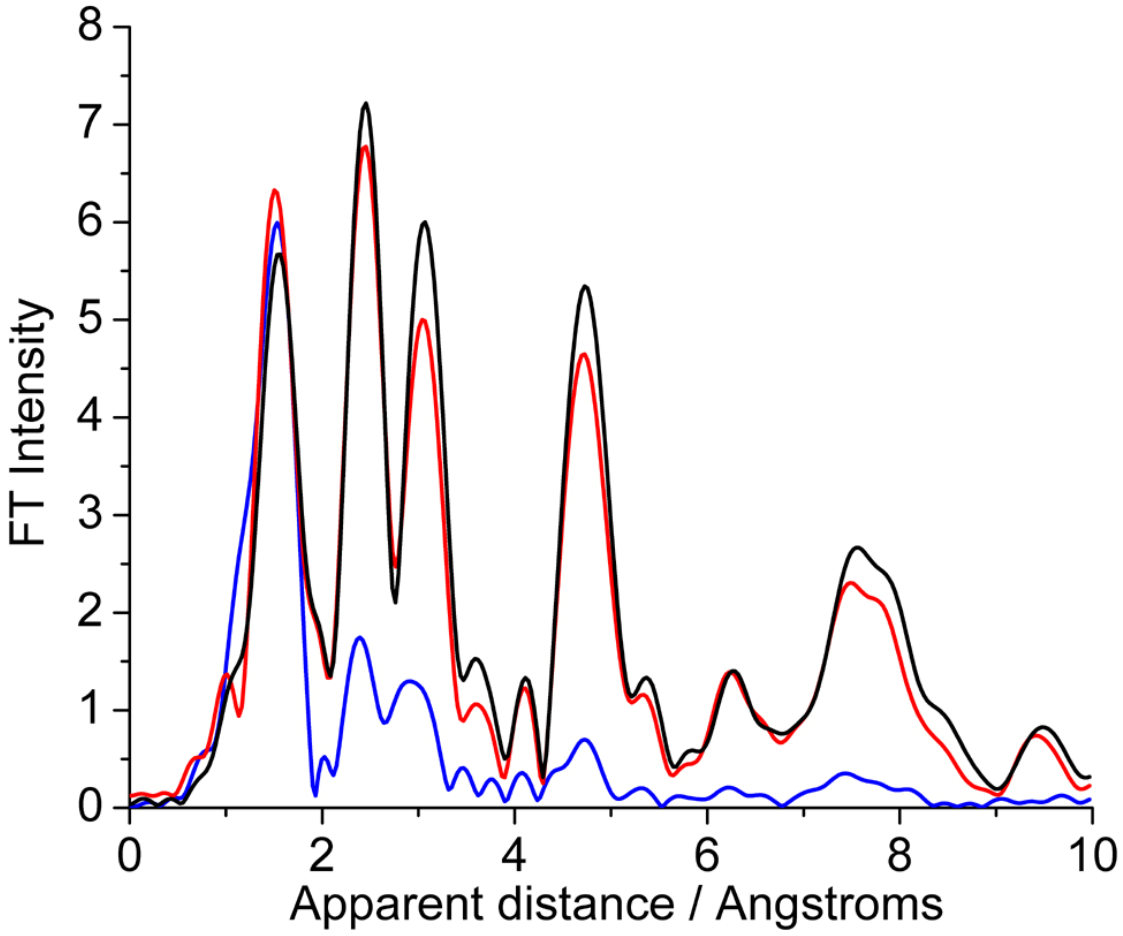

Figure 3: EXAFS spectra for bulk Co_3O_4 (black trace), SBA-15/Co_3O_4 (4%) (blue trace), and SBA-15/Co_3O_4 (8%) (red trace).

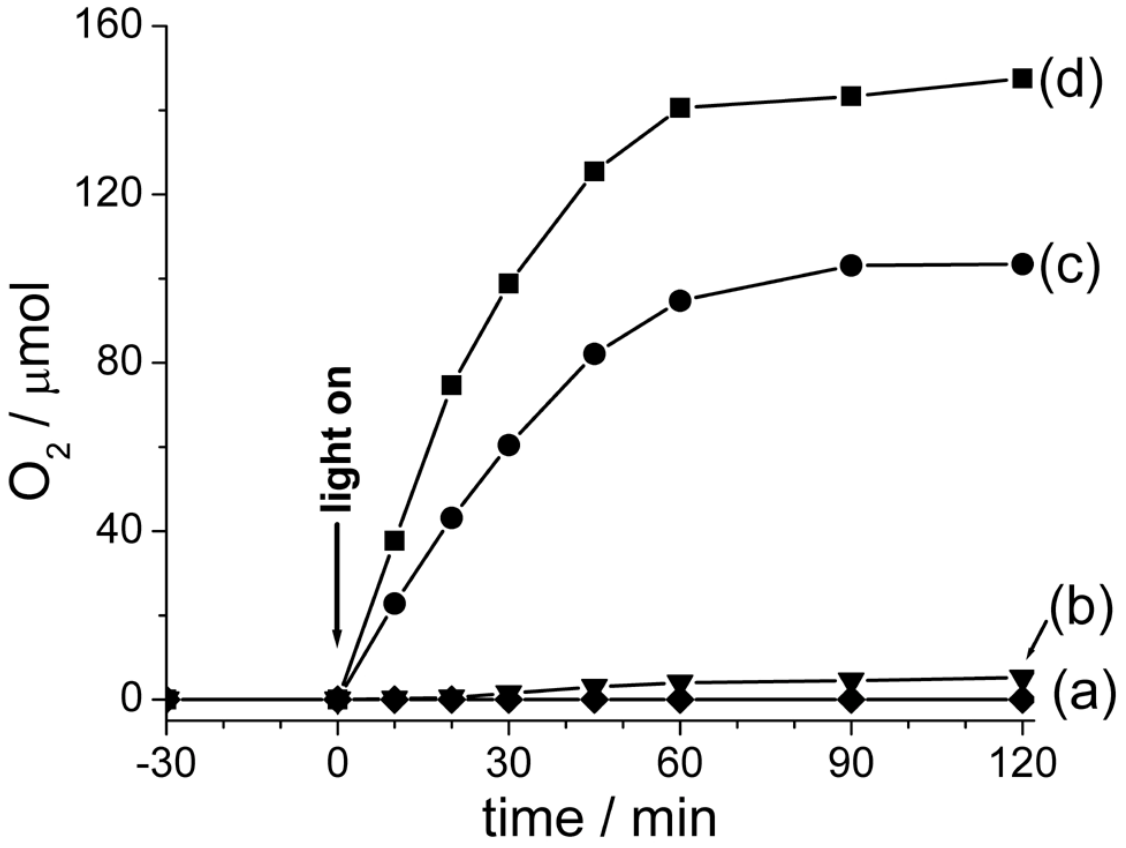

Figure 4: Oxygen evolution in aqueous suspensions (40 mL) of (a) SBA-15/NiO (8%), (b) micron-sized Co_3O_4 particles, (c) SBA-15/Co_3O_4 (8%), and (d) SBA-15/Co_3O_4 (4%). Measurements were conducted at pH 5.8 and 22 C. Catalysis was initiated by Ar ion laser emission at 476 nm (240 mW). Experimental details of the oxygen detection method are described in the Supporting Information.[12]